

## THE MANY STREAMS OF THE MAGELLANIC STREAM

SNEŽANA STANIMIROVIĆ<sup>1</sup>, SAMANTHA HOFFMAN<sup>1</sup>, CARL HEILES<sup>2</sup>, KEVIN A. DOUGLAS<sup>3</sup>, MARY  
PUTMAN<sup>4</sup>, JOSHUA E. G. PEEK<sup>2</sup>  
*Accepted by ApJ, February 2008*

## ABSTRACT

We present results from neutral hydrogen (HI) observations of the tip of the Magellanic Stream (MS), obtained with the Arecibo telescope as a part of the on-going survey by the Consortium for Galactic studies with the Arecibo L-band Feed Array. We find four large-scale, coherent HI streams, extending continuously over a length of 20 degrees, each stream possessing different morphology and velocity gradients. The newly discovered streams provide strong support for the tidal model of the MS formation by Connors et al. (2006), which suggested a spatial and kinematic bifurcation of the MS. The observed morphology and kinematics suggest that three of these streams could be interpreted as a 3-way splitting of the main MS filament, while the fourth stream appears much younger and may have originated from the Magellanic Bridge.

We find an extensive population of HI clouds at the tip of the MS. Two thirds of clouds have an angular size in the range  $3.5' - 10'$ . We interpret this as being due to thermal instability, which would affect a warm tail of gas trailing through the Galactic halo over a characteristic timescale of a few Myrs to a few hundred Myrs. We show that thermal fragments can survive in the hot halo for a long time, especially if surrounded by a  $< 10^6$  K halo gas. If the observed clumpy structure is mainly due to thermal instability, then the tip of the MS is at a distance of  $\sim 70$  kpc. A significant fraction of HI clouds at the tip of the MS show multi-phase velocity profiles, indicating the co-existence of cooler and warmer gas.

*Subject headings:* ISM: clouds — ISM: structure — radio lines: ISM

## 1. INTRODUCTION

The Magellanic Stream (MS), a  $10^\circ$  wide tail of neutral hydrogen (HI) emanating from the Magellanic Clouds and trailing for almost  $100^\circ$  on the sky ( $\text{Dec} \sim -60$  to  $+20^\circ$ ) (Wannier & Wrixon 1972; Mathewson et al. 1974), is the only clear example of a gaseous halo stream in the Milky Way's close proximity. While it is well accepted that the MS is the result of interactions between the Milky Way (MW) and the Magellanic Clouds, the relative importance of tidal stripping and various kinds of gasdynamical interactions is still very much under debate. Most recently several new attempts were made to model the observed HI column density and velocity distribution as being due to purely tidal stripping (Connors et al. 2006), or gravitational + hydrodynamical interactions (Mastropietro et al. 2005). These models focus on reproducing general features in the Magellanic System, and gradients in HI column density and velocity along the MS. To add more excitement to this topic, recent estimates of the proper motion of the Small Magellanic Cloud (SMC) by Kallivayalil et al. (2006) and the most recent calculations of the Magellanic Cloud's orbits by Besla et al. (2007) suggest, contrary to all previous studies, that the Clouds are only on their first passage around the MW. The new orbits imply that neither tidal nor ram pressure stripping would have had enough time to produce the MS, calling for alternative formation mechanisms.

The distance to the MS, especially to its tip, or the region the farthest away from the Magellanic Clouds, is

another contentious question and varies greatly between models. Under the ram pressure hypothesis the tip has fallen the farthest toward the MW and is at a distance of only 25 kpc. Early tidal models (Gardiner & Noguchi 1996; Yoshizawa & Noguchi 1999) place the tip at a distance of 60-70 kpc. The latest tidal simulations (Connors et al. 2006) find an even more distant component extending from 170 to 200 kpc. The latest orbit calculations (Besla et al. 2007) would also imply a significantly large distance to the MS,  $\sim 150$  kpc, although it is not clear where exactly the MS is relative to the Clouds in this framework.

For many years the MS was viewed as a complex of six discrete concentrations (labeled as MS I to VI). New HI Parkes surveys by Putman et al. (2003) and Brüns et al. (2005), with an angular resolution of  $15.5'$ , revealed a more complex nature of the MS gas, with a fascinating network of filaments and clumps. Two large spatial filaments were found to run in parallel over most of the MS length. Around  $\text{Dec} \sim 0^\circ$  the dual filaments disperse into many small clumps and filaments culminating in a chaotic appearance at the tip. The only high resolution view of two selected regions at the tip of the MS was by Stanimirovic et al. (2002) who used the Arecibo telescope to image two small regions in MS V ( $\text{Dec} \sim 8^\circ$ ) and MS VI ( $\text{Dec} \sim 12^\circ$ ). This work showed that the MS clumps have a complex morphology at  $3.5'$  resolution, strongly suggestive of interactions between the MS and an external medium. While most previous studies thought that the MS dissipates at its tip ( $\text{Dec} \sim 0^\circ$ ), very sensitive West-

<sup>1</sup> Department of Astronomy, University of Wisconsin, Madison, WI 53706; sstanimiro@astro.wisc.edu, shoffman3@wisc.edu

<sup>2</sup> Department of Astronomy, UC Berkeley, 601 Campbell Hall, Berkeley, CA 94720; goldston@astro.berkeley.edu

<sup>3</sup> Space Sciences Laboratory, University of California, Berkeley, CA 94720; douglasssl@berkeley.edu

<sup>4</sup> University of Michigan, Department of Astronomy, 500 Church St., Ann Arbor, MI 48109; mputman@umich.edu

erborn observations by Braun & Thilker (2004) suggested that the MS remarkably extends further to the north all the way to Dec  $\sim 40^\circ$ .

Another interesting phenomenon brought to light by the Parkes surveys is the presence of numerous small HI clumps which surround the main MS filaments in position and velocity (Putman et al. 2003). While the origin of these clumps is still unclear, several possible mechanisms have been invoked: the clumpiness in the original gas drawn out of the Magellanic Clouds, the instabilities along the MS's edge, or dense condensations within an extended mainly ionized MS component. One of the crucial issues about the origin and structure of the MS in general, is to what extent interactions with the MW halo determine or influence the MS gas. This problem becomes particularly important at the extreme northern end of the MS, because this portion of the MS is considered to be the oldest and has been immersed in the hot MW halo for a long time.

In this paper we present results from the recent HI observations of the tip of the MS obtained with the Arecibo telescope<sup>5</sup> as part of the on-going survey by consortium for Galactic studies with the Arecibo L-band Feed Array (GALFA). In Section 2 we briefly outline our observing and data processing methods. Section 3 describes several new filaments discovered at the tip of the MS, while in Section 4 we present a statistical summary of properties of numerous HI clouds found in this region. In Section 5 we discuss the origin of the MS and its clumpy structure based on our observations and results.

## 2. OBSERVATIONS AND DATA PROCESSING

The observations were conducted with the Arecibo telescope. GALFA HI survey consists of many individual projects. The data presented in this paper represent a combination of three GALFA projects: TOGS (or ‘Turn-On GALFA Spectrometer’ being undertaken in parallel with the ALFALFA extragalactic survey, PI: Putman), a2172 (PIs: Heiles & Peek, whose original target was a shell-like structure at Galactic velocities), and a2032 (PI: Stanimirovic, which observed a small region at the MS tip).

As general GALFA observing and data reduction strategies are summarized in Stanimirović et al. (2006), we emphasize here only a few important points. All observations were obtained with the dedicated spectrometer GALSPECT which has a fixed velocity resolution of 0.18 km s<sup>-1</sup>. For a2032 and a2172, the telescope was driven in the basket-weave mode producing inter-woven zig-zag scans in the RA-Dec coordinate frame. For TOGS, numerous drift scans along right ascension were made, as this is the preferred observing strategy for the ALFALFA survey (Giovanelli et al. 2005). Before each observing scan about 5 minutes were spent running ‘The Least-Squares Frequency Switching’ calibration procedure (Heiles 2007) which allows us to derive a reference spectrum to be applied to all spectra within the given scan.

We have then combined scans from TOGS (the ‘Fall’ session) and a2172 to obtain the data cube that covers a region  $37.5^\circ \times 24^\circ$  in size. Various zig-zag and drift scans

cross in many places. The crossing points were used to compare spectra and fine-tune our calibration. This procedure removes small gain offsets between adjacent drift scans and produces a resultant image mostly free of striping artifacts. After this fine-tuning, spectra from the two projects were gridded into a data cube. In the case of a2032 observations our strategy was different. After basic calibration, we have produced an a2032 data cube, and then added it linearly (in the image domain) to the combined TOGS+a2172 cube. Both combination processes worked very well. The images presented in this paper are the first demonstration of how successfully we can piece together data from different GALFA projects.

The only problem encountered during the data reduction is radio interference present in several TOGS scans at high negative LSR velocities. This interference affects all ALFA beams, varies across a given scan, and is centered around 1422 MHz. It is caused by a still unidentified source. We have edited affected scans where possible, however some artifacts are still noticeable in several images. Our future software developments will be better able to deal with this, and similar problems.

As the integration time was different for the three observing projects, our sensitivity varies across the image. ALFALFA and TOGS cover the sky twice with about 15 sec of integration time per beam, while a2172 and a2032 observations were obtained in a fast-scanning mode with an integration time of only about 5 sec per beam. Declination bands from  $11^\circ$  to  $16^\circ$  and  $24^\circ$  to  $28^\circ$  have the lowest rms noise level, 0.03 K per 1.4 km s<sup>-1</sup> wide channels. The rest of the image is noisier, with about 0.06-0.07 K per 1.4 km s<sup>-1</sup> wide channels. Our best 3- $\sigma$  sensitivity is  $3.3 \times 10^{18}$  cm<sup>-2</sup> over 20 km s<sup>-1</sup>.

## 3. FOUR FILAMENTS AT THE TIP OF THE MS

Figure 1 shows HI images from the final data cube at several selected velocities. In Figure 2 we show the first moment image, or the intensity-weighted velocity along the line-of-sight. The area covered in our observations is huge — about 870 square degrees ( $65^\circ < l < 105^\circ$ ,  $-54^\circ < b < -20^\circ$ ), focusing on the very tip of the MS where the two traditional MS filaments were found to be significantly spatially bifurcated (one is located at RA  $23^h 30^m$ , and the other one at RA  $\sim 23^h 00^m$ ). The only previous high resolution observations of about 10 square degrees within this region were obtained by Stanimirovic et al. (2002).

As Figures 1 and 2 show, several coherent HI filaments extend all the way to Dec  $\sim 25^\circ$ . Braun & Thilker (2004) reported an extension of the two MS filaments, in the form of diffuse gas, from Dec =  $20^\circ$  to  $40^\circ$ . We confirm the continuous extension of the MS from Dec =  $5^\circ$  to  $\sim 25^\circ$ . Beyond this point our observations may not be sensitive enough to detect a very low-column-density emission found by Braun & Thilker (2004). Our sensitivity of  $3 \times 10^{18}$  cm<sup>-2</sup> (over 20 km s<sup>-1</sup>) is significantly worse than Braun & Thilker (2004)'s lowest contour (in their Figure 5) shown at  $3 \times 10^{17}$  cm<sup>-2</sup>. However, the picture of the two interwoven filaments changes dramatically in our observations: instead of two traditional filaments we find several!

<sup>5</sup> The Arecibo Observatory is part of the National Astronomy and Ionosphere Center, operated by Cornell University under a cooperative agreement with the National Science Foundation.

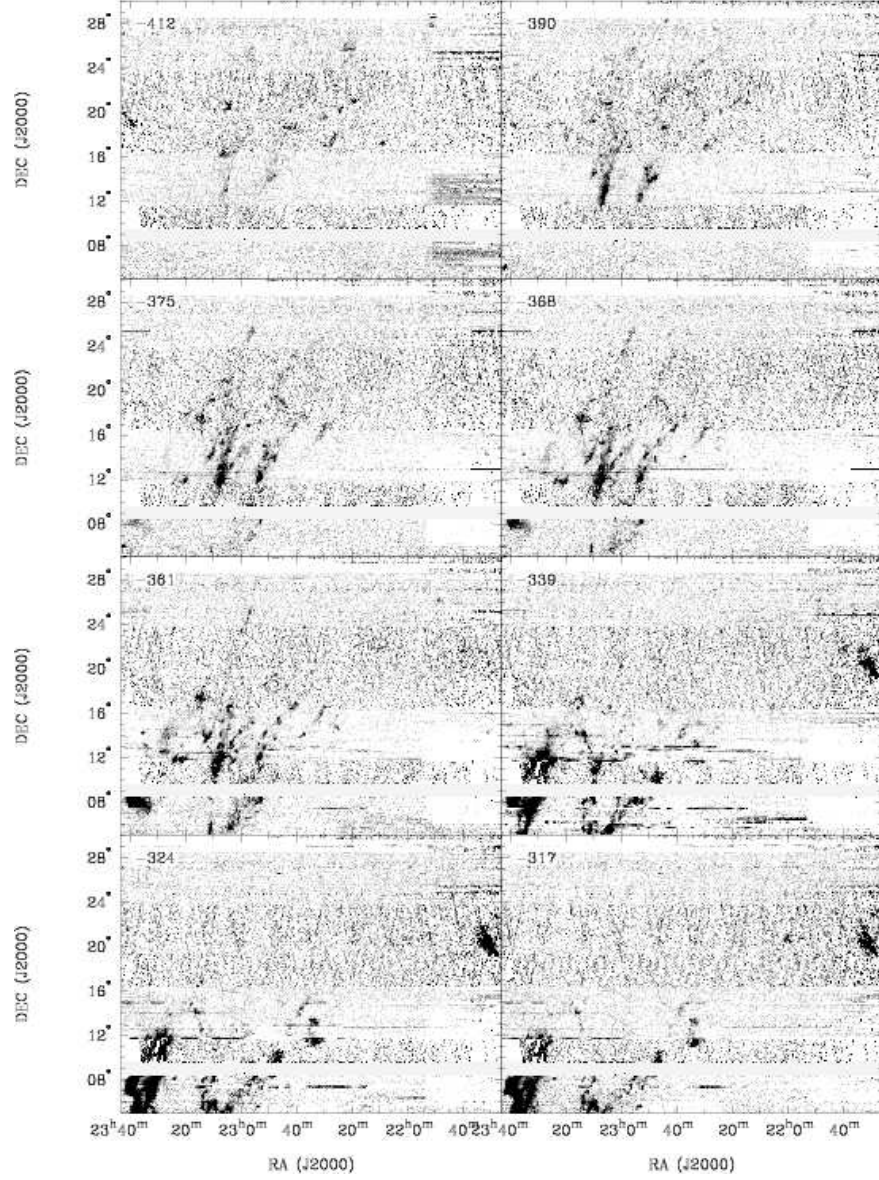


FIG. 1.— Right ascension-declination images of HI emission at the tip of the MS for different LSR velocities, given in the top left corner of each panel. The gray-scale intensity range is 0.005 to 0.15 K, with a linear transfer function. Several horizontal strips around  $\text{Dec} = 6^\circ$  and  $13^\circ$ , especially noticeable at lower negative velocities, are due to interference. The gap between  $\text{Dec} \sim 8^\circ$  and  $10^\circ$  is due to lack of data in this region. The zig-zag pattern noticeable in regions with a higher noise level is due to our scanning technique.

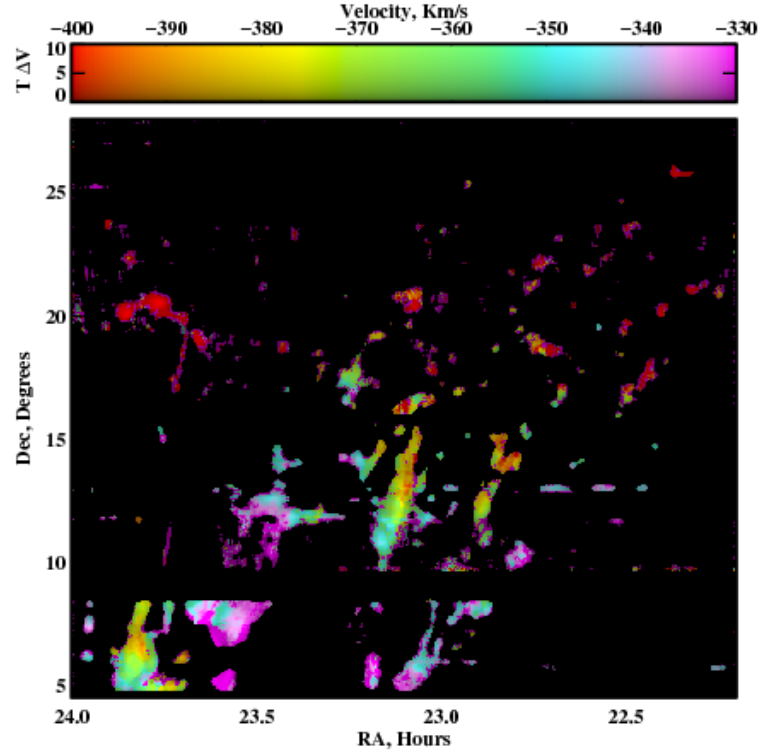


FIG. 2.— First moment image, or the velocity field, of the MS tip. Color represents the velocity centroids and brightness represents integrated intensity. The image has been smoothed to emphasize weak features.

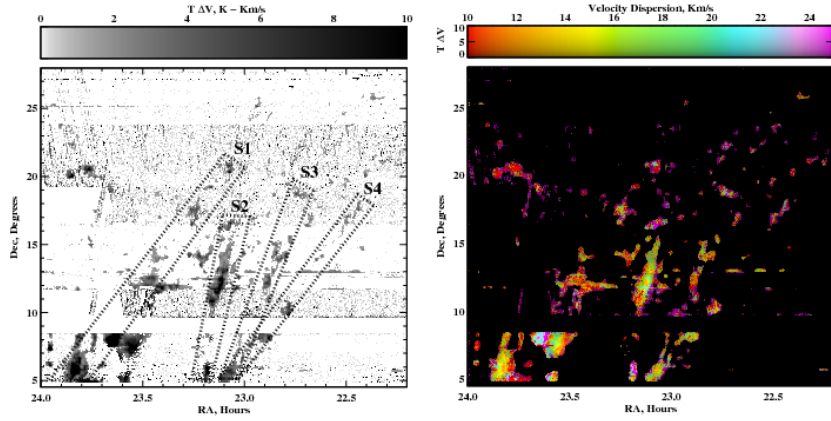


FIG. 3.— (left) An HI integrated intensity image with schematic representation of the four filaments. (right) Second moment or velocity dispersion.

While filaments often break into numerous branches and small clouds when viewed with Arecibo's resolution, there are at least four prominent and coherent large-scale structures noticeable across the whole velocity range. To facilitate further discussion we define and label filaments in the following way. Starting from the lowest negative velocities ( $\sim -320 \text{ km s}^{-1}$ ) in Figure 1:

1. 'S1' is centered at RA  $23^{\text{h}} 35^{\text{m}}$ , this is a portion of one of the two traditional MS filaments;
2. 'S2' is centered at RA  $23^{\text{h}} 10^{\text{m}}$  and can be traced through the whole velocity range;
3. 'S3' is centered at RA  $23^{\text{h}} 05^{\text{m}}$  and starts at a higher negative velocity of  $-360 \text{ km s}^{-1}$ ;
4. 'S4' starts at RA  $23^{\text{h}} 00^{\text{m}}$  and extends to RA  $22^{\text{h}} 35^{\text{m}}$ .

Figure 3 (left) shows a schematic representation of the four streams. Both S1 and S4 can be seen from the lowest negative velocities up to about  $-370 \text{ km s}^{-1}$ . S2, S3 and S4 seem to have spatially a common point of origin, and are most likely related to the second traditional MS filament. The morphology of the four streams is significantly different: S2, S3 and S4 consist of and are surrounded by numerous small, compact clumps, having a beads-on-string appearance. The number of compact clumps peaks at velocities  $-350$  to  $-370 \text{ km s}^{-1}$ . S1 on the other hand has a more diffuse morphology and contains the smallest number of compact clumps. This may indicate that S1 has a different origin relative to the other three streams, or that it is younger and therefore did not have enough time to fragment. We get back to this issue in Section 5.

While generally clumpy morphology is prominent, the four defined streams are coherent structures, which can be seen most clearly in the first moment image, Figure 2. All four streams show clear velocity gradients, although not all gradients are similarly steep. In Figure 4 we show position-velocity images along the streams. S1 and S3 have a velocity gradient of about  $5 \text{ km s}^{-1} \text{ deg}^{-1}$  over a length of 15 degrees, in agreement with the overall velocity gradient along most of the MS (Putman et al. 2003). S2 has the steepest gradient of almost  $10 \text{ km s}^{-1} \text{ deg}^{-1}$  along the first 10 degrees, and then it almost turns over in velocity roughly staying around  $-380$  to  $-400 \text{ km s}^{-1}$ . S4 has almost a constant velocity of  $\sim -340 \text{ km s}^{-1}$ . All streams have a similar velocity dispersion,  $\sim 15\text{-}20 \text{ km s}^{-1}$ , see Figure 3 (right). This is in agreement with Brüns et al. (2005) who measured a dispersion of  $15 \text{ km s}^{-1}$  along most of the MS.

#### 4. COMPACT HI CLOUDS AT THE TIP OF THE MS

A striking result from the above figures is the presence of numerous small HI clouds. The smallest clouds have a size down to our resolution limit of  $3.5'$  and are unresolved. Most of the clouds are compact and round, head-tail morphology is surprisingly uncommon. Previously, Putman et al. (2003) noticed two types of clouds which surround the MS along its southern portion: head-tail clouds with tails pointing along the major axis of the MS (typically, the head has a column density of  $10^{19} \text{ cm}^{-2}$  while the tail is 3-4 times fainter), and ubiquitous dense

HI clouds which follow the main MS filaments in position and velocity, some again with a head-tail morphology.

#### 4.1. Cloud catalog

We have compiled a catalog of 180 HI clouds. The positions of all clouds are shown in Figure 5. Clouds were selected by eye from the spectral line data cube. The integrated intensity image was used as a guide for cloud selection, local peaks in this image were considered as potential cloud candidates. We then used the full data cube to follow potential clouds spatially and in velocity, and measure cloud properties. Special care was taken to avoid breaking larger clouds into separate entities, however the catalog may still be slightly biased toward smaller clouds. We have made several checks to ensure cloud reliability and to exclude clouds potentially affected by scanning artifacts or RFI. There were several cases (mainly at low Dec) where multiple clouds are present along the line-of-sight at clearly different velocities. These cases were treated as individual clouds.

For each cloud we have measured the cloud size, the central velocity, and the peak HI column density. In addition, at the center of each cloud we have fitted the HI velocity profile with one or two Gaussian functions. Although the cloud catalog is not 100% complete, as it is hard to select clouds in the regions with higher noise, it certainly represents well the cloud population whose physical properties we want to study. Basic cloud properties are presented and discussed in the following sub-sections.

To ensure that we are dealing only with clouds of Magellanic origin, our cloud catalog was cross-correlated with the catalog of HVCs by Wakker & van Woerden (1991), the catalog of HVCs and CHVCs by de Heij et al. (2002), and the catalog of recently discovered mini-HVCs by Hoffman et al. (2004). HVCs come with a wide range of sizes and properties. While some represent large complexes, like the MS, most are smaller with sizes of a few tens of degrees. On the other hand, CHVCs represent a class of HVCs which are compact (with sharp edges in the HI column density distribution), apparently isolated from larger complexes, and with angular size less than  $2^\circ$ . One interpretation is that CHVCs are essentially the same as HVCs but located at much greater distances. Recently discovered mini-HVCs are even smaller and have diameters of  $9'$  to  $35'$ . These clouds are also more diffuse than typical HVCs, having the peak HI column density of only  $3 \times 10^{18} \text{ cm}^{-2}$ . Several of mini-HVCs were found to be superimposed on the northern extension ( $\text{Dec} > 0^\circ$ ) of the MS but at velocities distinct from those of the MS gas. One suggestion is that these clouds represent outliers of the MS complex (Hoffman et al. 2004).

There are 8 HVCs from Wakker & van Woerden (1991) in our field of view. Three HVCs are clearly detected and identified as clouds in our catalog, these are WvW413, WvW491 and WvW485. Additional three HVCs (WvW508, WvW492 and WvW472) have clouds nearby but at an angular separation larger than the beam of the Leiden-Dwingeloo survey. There are 19 HVCs and 3 CHVCs from de Heij et al. (2002) in our field of view. All of these CHVCs were detected.

As CHVCs were classified as isolated clouds it will be surprising to find a large population of CHVCs in our

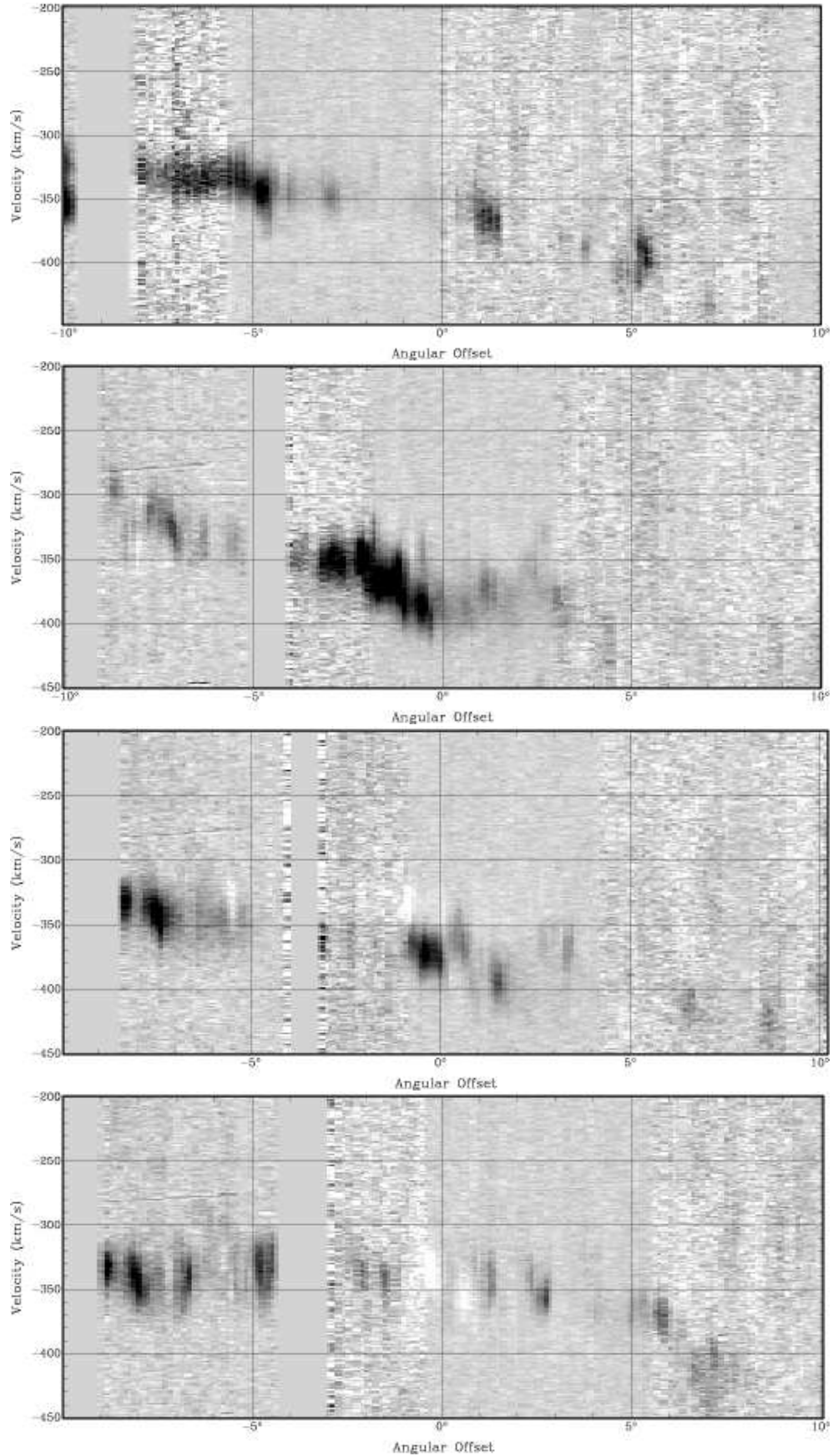


FIG. 4.— Position-velocity images along the four streams: S1, S2, S3, and S4 (top to bottom). This figure can be compared with Figure 9 from Connors et al. (2006).

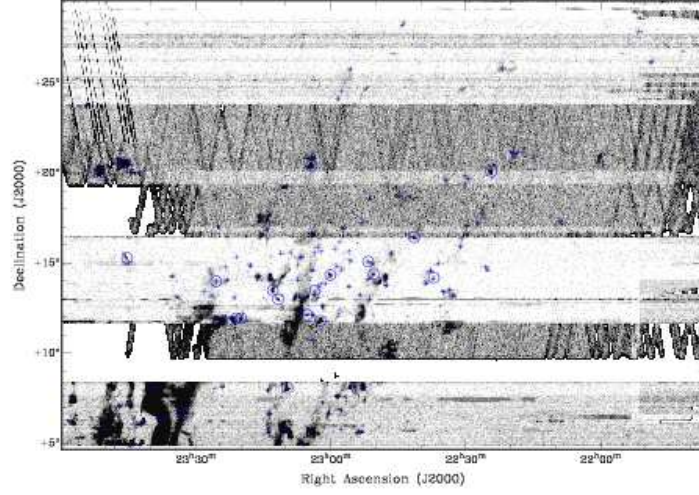


FIG. 5.— A peak brightness temperature image of the whole region with cataloged clouds. Clouds without multi-phase structure are shown as crosses, while clouds with multi-phase structure are shown as circles. See Section 4.2.

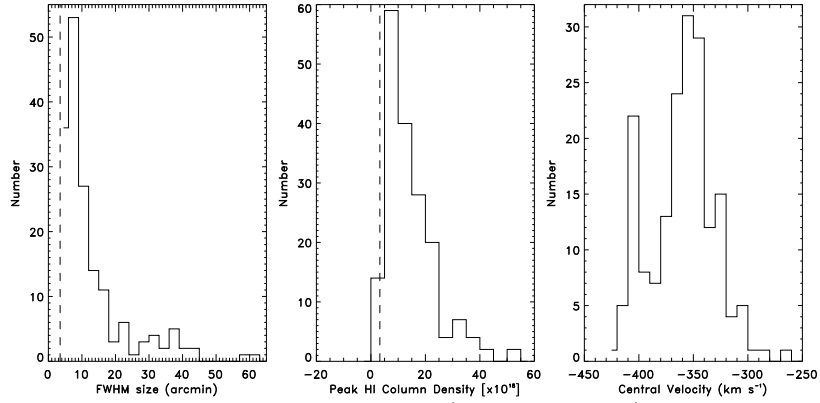


FIG. 6.— Histograms of measured cloud properties: cloud angular size (FWHM in arcmin), the peak HI column density (in  $10^{18} \text{ cm}^{-2}$ ), and the central LSR velocity. The dashed line in the left panel shows the angular resolution limit, while the dashed line in the middle panel shows the  $3\text{-}\sigma$  sensitivity limit of the survey.

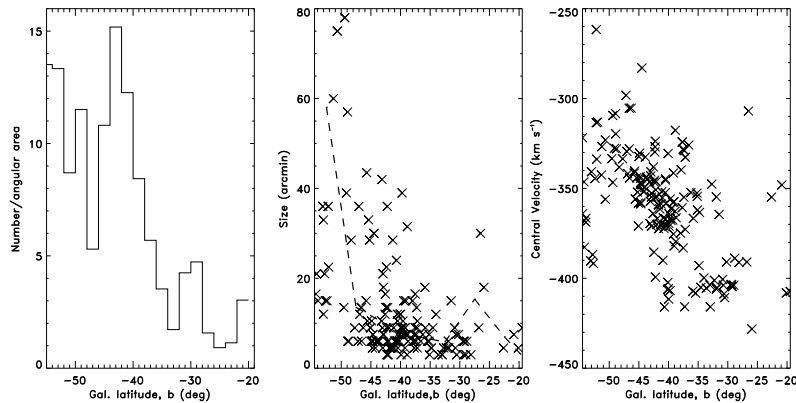


FIG. 7.— (left) Number of clouds as a function of Galactic latitude divided by the angular area observed at each latitude. (middle) Cloud size as a function of Galactic latitude. Dashed line represents a median value for each latitude bin. (right) Cloud central velocity as a function of Galactic latitude. In the case of clouds with multi-phase structure, the mean velocity is plotted.



cloud catalog. Only 3 CHVCs from de Heij et al. (2002) are in our field of view. CHVC229 (from de Heij et al. 2002) is extended and was found to be associated with several of our clouds at very low negative velocities ( $\sim -330$  km s $^{-1}$ ). We have excluded those HI clouds from our further analyses as at  $\sim -330$  km s $^{-1}$  these clouds are clearly spatially located far away from the MS emission.

Three mini-HVCs are in our field of view: LMPU 387-230, LMPU 387-275, and LMPU 387-297. LMPU 387-275 and LMPU 387-297 are at velocities ( $-275$  and  $-297$  km s $^{-1}$ , respectively) where we detect several small clumps, the closest one being about  $24'$  away. We did not detect LMPU 387-230 however, although Hoffman et al. (2004) estimated its HI column density to be  $4.8 \times 10^{18}$  cm $^{-2}$ , clearly above our detection limit.

In summary, we do not find that our catalog is contaminated by a significant population of CHVCs, it therefore contains primarily clouds associated with the MS.

## 4.2. Cloud properties

### 4.2.1. Cloud size, HI column density, and HI mass

Figure 6 shows histograms of cloud basic properties: angular size, HI column density, and central (LSR) velocity. The observed cloud angular size distribution strongly peaks around  $10'$ . 90% of clouds have a size in the range  $3'$  to  $35'$ . The abundance of very small, compact-looking clouds is significant, more than half of clouds in the catalog have an angular size less than  $10'$ . Obviously, these clouds would have been missed in previous large-scale surveys such as the Leiden-Argentine-Bonn (LAB) survey (Kalberla et al. 2005; Hartmann & Burton 1997; Bajaja et al. 2005; Arnal et al. 2000), or even Parkes surveys of the MS. The low-size cut-off of the histogram is clearly affected by our resolution limit of  $3.5'$ , and higher resolution observations will probably find many smaller clouds.

The cloud central HI column density distribution peaks around  $1.3 \times 10^{19}$  cm $^{-2}$ , 90% range is  $2.5 \times 10^{18}$  to  $3.2 \times 10^{19}$  cm $^{-2}$ . This distribution function is affected by our sensitivity limit, deeper observations will probably find many clouds with lower HI column density. For comparison, the HI column density distribution of mini-HVCs peaks at  $3 \times 10^{18}$  cm $^{-2}$ .

Figure 7 (left) shows that the number of clouds decreases steeply along the MS, in the direction toward the tip. The number of clouds in each latitude bin has been divided by the observed angular area to account for different areal coverage across the image. Figure 7 (middle) shows a tendency for clouds with angular size larger than  $20'$  to be found closer to the Magellanic Clouds (at  $b < -40^\circ$ ), while clouds with angular size less than  $20'$  appear along the whole latitude range. This could be interpreted as evidence that part of the MS with  $b < -40^\circ$  is at a larger distance, in agreement with tidal models. Please note that the gap around  $b = -25^\circ$  on this plot is due to the lack of clouds, not due to the lack of data in this region.

To provide an example of cloud linear size, HI mass, volume density, and thermal pressure, we use an angular diameter of  $10'$  and a median peak HI column density of  $1.3 \times 10^{19}$  cm $^{-2}$ , for three representative distance values, 20, 60, and 150 kpc, see Table 1.

### 4.2.2. Cloud central velocity

Interestingly, the cloud central velocity, shown in Figure 6 (right), shows a clear dichotomy. There are two peaks centered at  $-406$  and  $-351$  km s $^{-1}$ , with the velocity FWHM of 10 and 45 km s $^{-1}$ , respectively. As shown in Figure 7 (right), the velocity dichotomy manifests in the way that there are two main groups of clouds, one around  $b = -47^\circ$  to  $-37^\circ$  (or Dec =  $10^\circ$ - $15^\circ$ ) and  $v = -350$  km s $^{-1}$ , and the other one around  $b = -35^\circ$  to  $-27^\circ$  (Dec =  $18^\circ$ - $25^\circ$ ) and  $v = -400$  km s $^{-1}$ . This figure also shows an almost continuous linear decrease in velocity (from  $-300$  to  $-420$  km s $^{-1}$ ) with Galactic latitude. This is in agreement with the general velocity trend along the MS.

The observed velocity dichotomy may indicate a kinematic bifurcation of the MS tip. Such bifurcation would not be surprising. N-body simulations by Connors et al. (2006) found two kinematically separate components, one that follows closely the orbit of the LMC and has a lower negative velocity, and the other one with a more negative velocity. While separated kinematically, both components occupy the same  $(l, b)$  range.

### 4.2.3. Clouds with multi-phase structure

About 20% of the clouds in our catalog have velocity profiles whose fitting requires two Gaussian functions. This is indicative of the existence of a multi-phase medium. However, some of these velocity profiles could be due to the existence of multiple clouds along the line of sight, whose velocity profiles partially overlap. To account for this effect, we accept as multi-phase clouds only those which have a subsonically moving core and a warmer envelope. This criterion translates into the requirement that the absolute difference between the centers of the two fitted Gaussian functions does not exceed  $0.7 \times$  the FWHM of the broad component. Our final sample of multi-phase clouds contains 21 entries. As an example, in Figure 8 we show velocity profiles of ten multi-phase (the first two rows), and five clouds with a single Gaussian profile (the last row). In most multi-phase cases, a narrow Gaussian component fits the line center, while a broader Gaussian function is needed to fit the line wings.

Narrow line profiles were scarcely found in the MS in previous studies. Brüns et al. (2005) found one cloud with a velocity FWHM of only 4 km s $^{-1}$ , at  $l = 93.6^\circ$ ,  $b = -53.7^\circ$ . Kalberla & Haud (2006) used the LAB survey and decomposed all HI velocity profiles into Gaussian components. They found that the portion of the MS close to the Magellanic Clouds (and with positive velocities) has 27% of the sight lines with a narrow velocity component, while the portion further away from the Clouds (with negative velocities) has a significantly lower fraction, only about 10%. The lower number of narrow components was attributed to either a lower halo pressure and/or a larger distance of the northern MS extension. Our final fraction of multi-phase clouds (12%) is similar to Kalberla & Haud's estimate for the negative velocity portion of the MS.

Figure 9 (left) shows the FWHM vs central velocity of all fitted Gaussian functions: crosses correspond to clouds with a single Gaussian component, while diamonds and circles represent the secondary (or narrow) and the pri-



TABLE 1  
CLOUD RADIUS, HI MASS, HI VOLUME DENSITY, AND THERMAL PRESSURE.

Distance (kpc)	Radius (pc)	HI mass ( $M_{\odot}$ )	HI volume density ( $\text{cm}^{-3}$ )	Pressure ( $\text{K cm}^{-3}$ )
20	30	$2 \times 10^2$	0.4	40
60	90	$2 \times 10^3$	0.1	10
150	220	$1 \times 10^4$	0.05	5

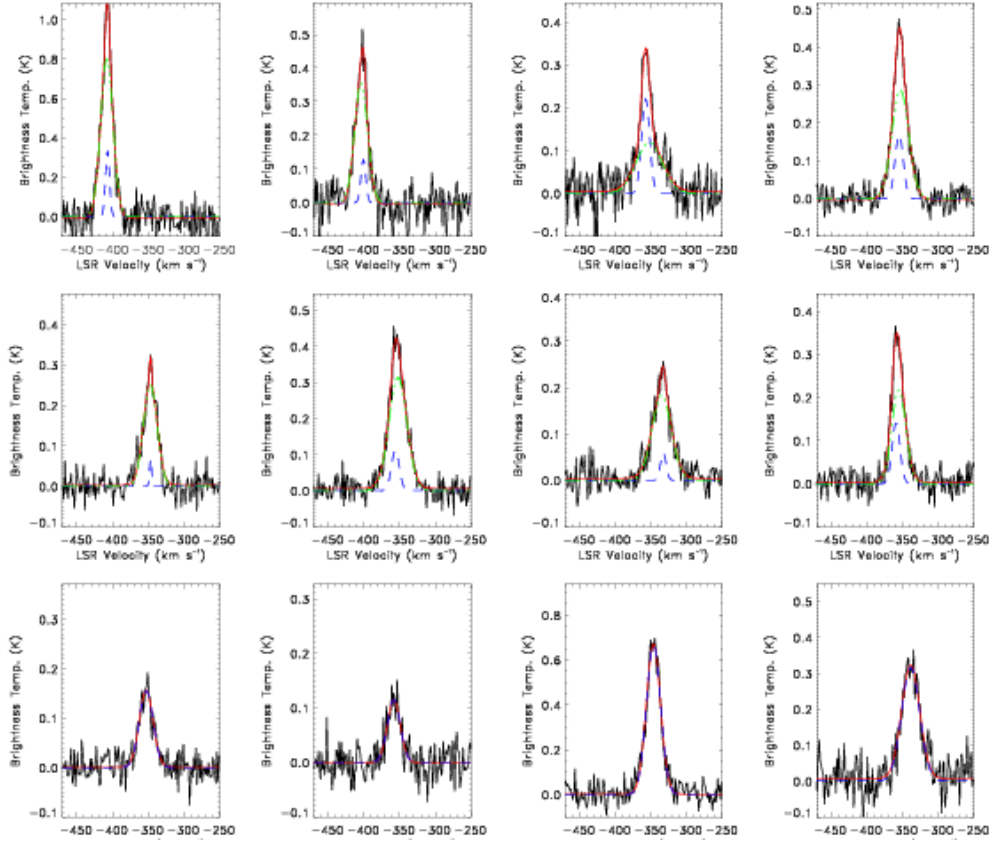


FIG. 8.— A few examples of HI clouds with and without multiple velocity components. The top two rows show clouds whose velocity profiles require two Gaussian functions, the bottom row shows a few clouds with just a single Gaussian velocity profile. For multiple velocity components, the broad velocity component is shown in green, the narrow component is shown in blue, and their sum is shown in red.

mary (or broad) velocity component for clouds with multi-phase medium. The FWHM of single-component clouds is predominantly in the range of  $20\text{--}30\text{ km s}^{-1}$ . For multi-phase clouds, the FWHM of the narrow component has a broad, almost continuous, range from  $3\text{ to }20\text{ km s}^{-1}$ , with a median value of  $13\text{ km s}^{-1}$ . This would imply an upper limit on the kinetic temperature in the range  $200\text{--}9000\text{ K}$ , mostly being in the thermally unstable regime. For comparison, Kalberla & Haud (2006) find the FWHM of the narrow component in the range  $5\text{--}28\text{ km s}^{-1}$ . The FWHM of the broad component of multi-phase clouds is around  $25\text{ km s}^{-1}$ , in agreement with what is found for clouds with only a single Gaussian component.

The right panel in Figure 9 shows the central velocities for both types of clouds. The velocity dichotomy is still noticeable with two peaks around  $-405$  and  $-350\text{ km s}^{-1}$ . This shows that the velocity bifurcation affects both clouds with and without multi-phase structure. We return to this point in Section 5.2.4.

## 5. DISCUSSION

### 5.1. Origin of the MS filaments

There are several important observational points presented in the previous sections:

- there are four coherent streams at the tip of the MS;
- S1 is diffuse, while S2, S3 and S4 are clumpy;
- spatially, S2, S3 and S4 appear to originate from a similar location;
- the velocity gradient along streams gradually decreases from S2 to S4;
- there is a lack of large clouds at low Galactic latitudes;
- central velocities of clouds with and without multi-phase structure show velocity bifurcation at  $-350$  and  $-405\text{ km s}^{-1}$ .

Traditionally, it was assumed that the MS originated purely from the SMC gas. Putman et al. (2003) suggested that the two double-helix-like MS filaments could arise from gas stripped from the Magellanic Bridge and the SMC. By using the LAB survey of Galactic HI (angular resolution of  $0.6^\circ$ ), Nidever et al. (2007) were able to trace one of the two filaments all the way to an over-density region in the LMC.

The only numerical study that addressed spatial bifurcation of the MS is by Connors et al. (2006). These authors showed that gross features of the MS and the leading arm, as well as the spatial bifurcation of the main MS filament, can be reproduced purely by tidal interactions between the MW and the Magellanic Clouds. They also suggested that the main MS filament is broken into two kinematic components. Several distinct features are found in their simulation.

1. The main MS filament was created 1.5 Gyr ago in a major encounter between the SMC, the LMC, and the MW. Further tidal ‘kicks’ from encounters with

the LMC 1.05 and 0.55 Gyrs ago resulted in its spatial, and then kinematic bifurcation. While one of the bifurcated components follows the orbit of the Magellanic Clouds and has a lower negative velocity ( $\sim -350\text{ km s}^{-1}$ ), the other possesses a higher negative velocity ( $-500\text{ to }-400\text{ km s}^{-1}$ ).

2. In addition to the main stream, which extends in distance from  $60\text{ to } \sim 100\text{ kpc}$ , there is the third stream right at the tip which spatially coincides with the main stream but has distinct kinematics and is significantly further away (distance of  $170\text{ to }220\text{ kpc}$ ). This component was created in an encounter between the SMC and the LMC 2.2 Gyrs ago, and is the oldest and the most distant feature in the Magellanic System.
3. Two tidal tails were drawn  $< 200\text{ Myr}$  ago from the Magellanic Bridge and follow the main filament along most of its length.

By drawing a parallel with this simulation, streams S2, S3 and S4 could represent a 3-way splitting of the main MS filament. As we show in the next section, this gas has had enough time to cool and fragment and is therefore very clumpy. As suggested by the simulation, most of the spatial 3-way splitting could have occurred in the more recent past,  $1\text{ Gyr to }500\text{ Myr}$  ago, during close encounters between the MS and the LMC. The fact that S2 to S4 show a decreasing steepness in their velocity gradients may be suggesting that these filaments were separated in subsequent encounters. S1 on the other hand, may represent one of the more recently formed tidal tails, drawn out of the Magellanic Bridge  $< 200\text{ Myrs}$  ago. The fact that it is significantly less clumpy than the other three streams suggests that S1 may be significantly younger, and have not had enough time to cool and fragment.

The lack of large HI clumps at the higher Galactic latitude suggests that the far tip of the MS may be more distant. However, the fact that we find clumps with multi-phase structure almost along the whole latitude range implies that the far tip is probably not too distant. As discussed in the next section, it would be hard to justify the existence of multi-phase medium at a distance of  $\sim 200\text{ kpc}$ . Another disagreement with the simulation concerns the observed LSR velocity at the far tip, we find  $\gtrsim -420\text{ km s}^{-1}$ , while the simulation predicts velocities down to  $-500\text{ km s}^{-1}$ .

However, the observed large-scale filaments at the tip of the MS, as well as the evidence for kinematic bifurcation, give strong support to the tidal formation scenario for the MS. While the observations are only qualitatively in agreement with the simulations, and many details still have to be worked out, it is extremely encouraging to see that detailed spatial and velocity structure of the MS can be reproduced *purely* by tidal interactions. Better observed coverage of this region, as well as high resolution observations of the southern MS extension, will certainly help to constrain this and other possibilities in the future.

### 5.2. Origin of Compact clouds

At certain velocities the MS has a very clumpy morphology. One of the obvious questions is: what physical processes are responsible for such a clumpy structure?

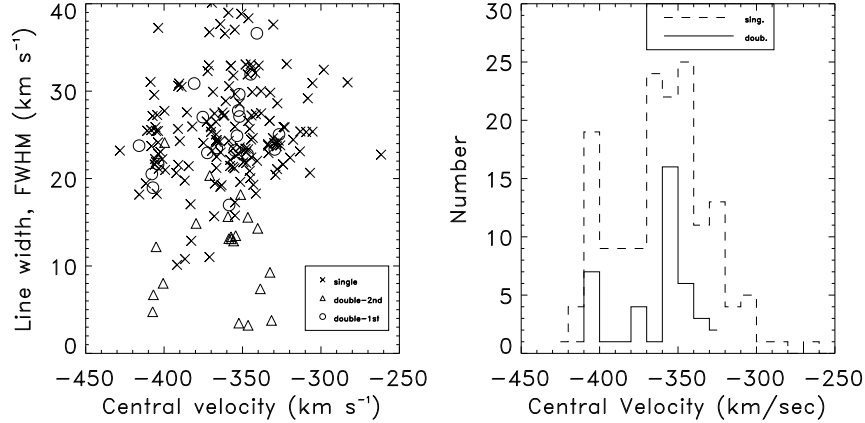


FIG. 9.— (left) Velocity FWHM vs central velocity for all fitted Gaussian functions. Crosses correspond to clouds with only one Gaussian component. Diamonds and circles show narrow and broad velocity component, respectively, in the case of clouds with multi-phase structure. (right) Histogram of central velocities for clouds with a single Gaussian function (dashed line), and clouds with two Gaussian functions (solid line). Central velocities of both Gaussian components were used to derive the solid-line histogram.

In trying to understand the cloud origin we look briefly into three important physical processes that would affect a tidal stream of warm gas moving through a hot ambient medium. All three processes have their characteristic time and spatial scales.

#### 5.2.1. Thermal instability

Thermal instability arises due to gas cooling and results in spatial fragments of the WNM, whose size is defined by the cooling length  $\lambda_{\text{cool}}$ . This process operates on the cooling timescale, defined by  $\tau_{\text{cool}} = kT_w/(\Lambda n_w)$ , with  $\Lambda$  being the cooling function,  $k$  being the Boltzmann constant, and  $T_w$  and  $n_w$  being the temperature and volume density of the WNM gas. If we consider a WNM gas that originated in the SMC, then  $n_w = 5 \times 10^{-2} \text{ cm}^{-3}$  (based on the size and total mass of the SMC, also measurements in (Stanimirović et al. 1999)), then for  $T_w = 8000 \text{ K}$  we estimate  $\lambda_{\text{cool}} \sim 100 - 200 \text{ pc}$  and the cooling timescale of  $\tau_{\text{cool}} \sim 20 - 30 \text{ Myr}$ . For a lower value of  $n_w$ , which is not unreasonable for the gas drawn out of the SMC outskirts, both  $\lambda_{\text{cool}}$  and  $\tau_{\text{cool}}$  will increase. Considering that most models suggest the MS age of 1-1.5 Gyr, thermal instability, with a typical timescale of a few tens to a few hundreds of Myrs, most likely have had a significant effect on the evolution of the MS gas.

Recent numerical simulations by Audit & Hennebelle (2005) provide an example of thermal condensation of warm gas. These simulations focus on a collision of incoming turbulent WNM flows and thermal condensation of WNM into colder gas. While not exactly applicable in our case, it is still very instructive to notice the properties of typical thermal fragments. A collision of incoming WNM streams creates a thermally unstable region, which partially condenses into cold clouds. The thermally unstable warm gas (with temperature of 200 – 5000 K) has a filamentary morphology and its fragmentation into cold clouds (with temperature < 200 K) is heavily controlled by turbulence. Cold clouds formed in simulations are thermally stable and long-lived, in the case of stronger turbulence they have round morphology, while a weaker turbulence is responsible for more elongated morphology of cold

clouds. The simulations show that the fraction of cold gas (with temperature < 200 K) produced in this process ranges from 10% in a strong turbulent case, to about 30% in a weak turbulent case. It is interesting to note that the lower bound on this CNM-to-WNM fraction agrees with the fraction of HI clouds with cool cores we find in our observations (12%).

#### 5.2.2. Kelvin-Helmholtz (KH) instability

Kelvin-Helmholtz (KH) instability occurs at the interface of the moving warm stream of gas and the ambient medium and also results in the formation of small fragments with a power-law size distribution. The timescale on which this instability develops,  $\tau_{\text{KH}}$  (given in Gyr), is given by:

$$\tau_{\text{KH}} = \frac{R_{\text{cl}} D_n^{1/2}}{v} \quad (1)$$

(Murray et al. 1993), where  $R_{\text{cl}}$  would be the initial size (radius) of the MS gas pulled out of the Magellanic Clouds,  $D_n = n_w/n_h$  corresponds to the density contrast of the warm KH fragments and the ambient hot medium, and  $v$  is the stream velocity. We use  $v = 220 \text{ km s}^{-1}$  (Stanimirović et al. 2002), assuming that the velocity of the original MS gas is equal to its present day velocity. We also assume that  $R_{\text{cl}} \sim 10^\circ$ , based on the size of the MSVI portion of the MS, and that this material was initially at a distance of 60 kpc.

If  $n_h = 10^{-4} \text{ cm}^{-3}$ , and  $n_w = 5 \times 10^{-2} \text{ cm}^{-3}$ , then  $\tau_{\text{KH}} \sim 600 \text{ Myr}$ . As this timescale is almost comparable to the age of the MS (in the framework of tidal and ram-pressure models), we can conclude that the KH instability has had a negligible effect on the evolution of the MS gas.

#### 5.2.3. Cloud evaporation

Once the warm stream has fragmented due to thermal/KH instability into smaller clouds, the third process becomes important — this is conductive heat transfer between the warm stream fragments and the hot ambient medium. Lin & Murray (2000) show that the size of the smallest fragments is set by the cloud ability to radiate away the energy flux due to conduction.

The warm clouds reside within warmer phases, hot halo gas with  $T_h \sim 10^6$  K and warm ionized gas with  $T_h \sim 10^5$  K. Detections of OVI absorption from gas associated with the MS Sembach et al. (2003) give strong support for the existence of an ionized component around the MS with  $T_h < 10^6$  K. It is expected that different phases are separated by an interface region through which heat flows between the two phases. The interface is a surface of transition where, for small clouds, the WNM evaporates into the warmer medium. The classical evaporation theory (McKee & Cowie 1977) predicts a critical radius for clouds at which radiative losses balance the conductive heat input, and at which the cloud neither evaporates nor condenses. Clouds smaller than the critical radius evaporate, while clouds larger than the critical radius accrete by condensation of the surrounding gas.

In the case of an interface between the WNM and the HIM, the cloud critical radius ( $R_{\text{rad}}$ ) times the density of the surrounding medium,  $n_h$ , is  $5 \times 10^{17} \text{ cm}^{-2}$  for  $T_h = 10^6$  K, or  $5 \times 10^{16} \text{ cm}^{-2}$  for  $T_h = 10^5$  K (from Fig. 2 in McKee & Cowie 1977). Generally, the expected critical radius decreases with increasing  $n_h$ . However, for  $n_h \sim 10^{-4} \text{ cm}^{-3}$ , the critical radius is large,  $R_{\text{rad}} \gtrsim 200$  pc. Clouds smaller than  $\sim 200$  pc would then evaporate, while WNM clouds larger than  $\sim 200$  pc would accrete the HIM by condensation. Thermal fragments we considered in Section 5.3 with a size  $\lambda_{\text{cool}} \sim 200$  pc will be predominantly smaller than the critical radius and therefore undergoing evaporation.

These small ( $\sim 200$  pc), evaporating clouds are surprisingly long-lived though. For mainly neutral clouds surrounded by the hot gas, the classical mass-loss rate is  $2 \times 10^{29} \text{ gr yr}^{-1}$  for  $T_h = 10^6$  K, or  $\sim 10^{27} \text{ gr yr}^{-1}$  for  $T_h = 10^5$  K (Slavin 2007). In the case of saturated evaporation the mass-loss rates are even lower. For  $n_w = 5 \times 10^{-2} \text{ cm}^{-3}$  the evaporation timescale is  $\tau_{\text{evp}} = 0.4$  Gyr for  $T_h = 10^6$  K, or  $\tau_{\text{evp}} = 80$  Gyr for  $T_h = 10^5$  K. But the timescales are in general long, approaching or being longer than 1 Gyr. We hence conclude that small fragments would be able to survive for a long time, at least a Gyr, most likely throughout the whole lifetime of the MS.

#### 5.2.4. Constraining cloud distances

As thermal instability must have played a very important role in the evolution of the oldest MS gas, we suggest that this could be the dominant process responsible for the clumpy structure found in our observations. The importance of thermal instability is further supported by the large abundance of small HI clumps (see Section 4.2.1). The KH instability is important as well, however it has a significantly longer timescale. As we have shown, it is reasonable to expect that thermal and/or KH fragments can survive for a long time, especially if surrounded by the ambient gas with  $T_h < 10^6$  K.

It is interesting that cloud morphology in our observations is dominated by round shapes. Elongated or head-tail clouds are surprisingly absent in our HI images. Head-tail morphology is commonly observed for CHVCs and is often seen as a signature of ram-pressure stripping, or other types of interactions between a cloud and the ambient halo medium. We therefore conclude that ram pressure effects probably have a secondary role, with gravitational forces being the dominant gas removal process.

If we assume that thermal fragmentation is the dominant process responsible for the clumpy structure, we can estimate a distance to the MS. If we assume that the median value of the cloud angular size distribution ( $10'$ ) corresponds to the linear size of ‘typical’ thermal fragments,  $\lambda_{\text{cool}} \sim 200$  pc (derived assuming  $n_w = 5 \times 10^{-2} \text{ cm}^{-3}$ ), we estimate a distance of  $\sim 70$  kpc. Please note that these numbers are only representative. The cloud angular size varies and is also affected by our resolution limit, the volume density of the warm MS gas is also not a constant number. However, this exercise is very instructive and demonstrates that thermal fragments can reasonably well explain at least some small-scale structure in the MS. The MS distance of  $\sim 70$  kpc is in agreement with the predictions from tidal models. Even more impressively, this distance agrees well with the recent estimate of 75 kpc by Jin & Lynden-Bell (2007), who used a geometrodynamical model and assumed that the MS follows a planar orbit around the Galactic center.

Also, the existence of multi-phase HI clouds can be used to place an upper limit on the MS distance. It is important to stress that the existence of multi-phase clouds along the tip of the MS, and especially at a distance of  $\sim 80$  kpc, is extremely surprising from a theoretical point of view. Based on the consideration of cooling and heating processes in an isothermal  $10^6$  K halo, Wolfire et al. (1995) predicted that multi-phase clouds, pressure confined by the hot halo, should exist in the MS only at distances less than 20 kpc from the Galactic plane. More recently, considering CHVCs Sternberg et al. (2002) showed that dark matter can provide an additional confinement mechanism, allowing the existence of multi-phase structure at distances  $\lesssim 150$  kpc. The multi-phase clouds at the tip of the MS therefore suggest that the tip is likely to be at a distance  $< 150$  kpc. This argues against the existence of the third, very distant stream found in the simulations by Connors et al. (2006), at least within the area covered by our observations. Also, as pointed out by Kalberla & Haud (2006), the multi-phase structure at the MS distance suggests a lower confining halo gas pressure than what is expected in the theoretical framework.

## 6. SUMMARY AND CONCLUSIONS

We have obtained HI observations of a region,  $\sim 900$  square degrees large, at the tip of the MS. The major results are as follows.

1. We find four coherent HI streams at the tip of the MS, extending continuously from Dec  $5^\circ$  to  $25^\circ$ . The streams have different morphology and velocity gradients. Three streams are very clumpy, while one stream is mainly made up of large diffuse structures.
2. The comparison of observations with the tidal simulations by Connors et al. (2006) suggests that the three clumpy streams could be a result of a 3-way tidal splitting of the main MS filament, induced by encounters between the LMC and the MS. The fourth stream is probably much younger, and could have been tidally drawn from the Magellanic Bridge in the more recent past,  $< 200 - 500$  Myr.

This stream is more diffuse because it has not had enough time to cool and fragment.

3. We find an extensive population of HI clouds at the tip of the MS. The smallest clouds have a size reaching down to our resolution limit of  $3.5'$ . 70% of clouds have an angular size in the range  $3.5' - 10'$ . About 12% of the MS clouds show multi-phase velocity profiles, indicating the co-existence of cooler and warmer gas. Cloud central velocities show two peaks at  $-350$  and  $-400$  km s $^{-1}$ .
4. We show that for warm gas trailing through the Galactic halo for the past Gyr or so, the effects of KH instability are relatively unimportant. However, thermal instability, with a typical timescale of a few Myrs to a few hundred Myrs, is significantly important and will result in the fragmentation of gas and the formation of smaller clumps. The ob-

served clumpiness at the tip of the MS could be fully or partially due to this mechanism.

5. We show that thermal/KH fragments can survive in the hot halo for a long time ( $> 1$  Gyr), especially if surrounded by a  $< 10^6$  K halo gas.
6. If the observed angular size of HI clumps is due to thermal instability, then the tip of the MS is at a distance of  $\sim 70$  kpc.

We are grateful to everyone at the Arecibo Observatory for their help in conducting these observations. It is a pleasure to acknowledge stimulating discussions with Fabian Heitsch, Bruce Elmegreen, Bob Benjamin, and Jay Gallagher. We thank an anonymous referee for constructive suggestions. Support by NSF grants AST-0097417 and AST-0707679 is gratefully acknowledged.

#### REFERENCES

- Arnal, E. M., Bajaja, E., Larrarte, J. J., Morras, R., & Pöppel, W. G. L. 2000, *A&AS*, 142, 35
- Audit, E. & Hennebelle, P. 2005, *A&A*, 433, 1
- Bajaja, E., Arnal, E. M., Larrarte, J. J., Morras, R., Pöppel, W. G. L., & Kalberla, P. M. W. 2005, *A&A*, 440, 767
- Besla, G., Kallivayalil, N., Hernquist, L., Robertson, B., Cox, T. J., van der Marel, R. P., & Alcock, C. 2007, *ArXiv Astrophysics e-prints*
- Braun, R. & Thilker, D. A. 2004, *A&A*, 417, 421
- Brüns, C., Kerp, J., Staveley-Smith, L., Mebold, U., Putman, M. E., Haynes, R. F., Kalberla, P. M. W., Muller, E., & Filipovic, M. D. 2005, *A&A*, 432, 45
- Connors, T. W., Kawata, D., & Gibson, B. K. 2006, *MNRAS*, 371, 108
- de Heij, V., Braun, R., & Burton, W. B. 2002, *A&A*, 391, 67
- Gardiner, L. T. & Noguchi, M. 1996, *MNRAS*, 278, 191
- Giovanelli, R., Haynes, M. P., Kent, B. R., Perillat, P., Saintonge, A., Brosch, N., Catinella, B., Hoffman, G. L., Stierwalt, S., Spekkens, K., Lerner, M. S., Masters, K. L., Momjian, E., Rosenberg, J. L., Springob, C. M., Boselli, A., Charmandaris, V., Darling, J. K., Davies, J., Lambas, D. G., Gavazzi, G., Giovanardi, C., Hardy, E., Hunt, L. K., Iovino, A., Karachentsev, I. D., Karachentseva, V. E., Koopmann, R. A., Marinoni, C., Minchin, R., Muller, E., Putman, M., Pantoja, C., Salzer, J. J., Scodeggio, M., Skillman, E., Solanes, J. M., Valotto, C., van Driel, W., & van Zee, L. 2005, *AJ*, 130, 2598
- Hartmann, D. & Burton, W. B. 1997, *Atlas of Galactic Neutral Hydrogen* (Atlas of Galactic Neutral Hydrogen, by Dap Hartmann and W. Butler Burton, pp. 243. ISBN 0521471117. Cambridge, UK: Cambridge University Press, February 1997.)
- Heiles, C. 2007, *PASP*, 119, 643
- Hoffman, G. L., Salpeter, E. E., & Hirani, A. 2004, *AJ*, 128, 2932
- Jin, S. & Lynden-Bell, D. 2007, *MNRAS*
- Kalberla, P. M. W., Burton, W. B., Hartmann, D., Arnal, E. M., Bajaja, E., Morras, R., & Pöppel, W. G. L. 2005, *A&A*, 440, 775
- Kalberla, P. M. W. & Haud, U. 2006, *A&A*, 455, 481
- Kallivayalil, N., van der Marel, R. P., & Alcock, C. 2006, *ApJ*, 652, 1213
- Lin, D. N. C. & Murray, S. D. 2000, *ApJ*, 540, 170
- Mastropietro, C., Moore, B., Mayer, L., Wadsley, J., & Stadel, J. 2005, *MNRAS*, 363, 509
- Mathewson, D. S., Cleary, M. N., & Murray, J. D. 1974, *ApJ*, 190, 291
- McKee, C. F. & Cowie, L. L. 1977, *ApJ*, 215, 213
- Murray, S. D., White, S. D. M., Blondin, J. M., & Lin, D. N. C. 1993, *ApJ*, 407, 588
- Nidever, D. L., Majewski, S. R., & Butler Burton, W. 2007, *ArXiv e-prints*, 706
- Putman, M. E., Staveley-Smith, L., Freeman, K. C., Gibson, B. K., & Barnes, D. G. 2003, *ApJ*, 586, 170
- Sembach, K. R., Wakker, B. P., Savage, B. D., Richter, P., Meade, M., Shull, J. M., Jenkins, E. B., Sonneborn, G., & Moos, H. W. 2003, *ApJS*, 146, 165
- Slavin, J. D. 2007, in *Astronomical Society of the Pacific Conference Series*, Vol. 365, *SINS - Small Ionized and Neutral Structures in the Diffuse Interstellar Medium*, ed. M. Haverkorn & W. M. Goss, 113
- Stanimirović, S., Dickey, J. M., Krčo, M., & Brooks, A. M. 2002, *ApJ*, 576, 773
- Stanimirović, S., Putman, M., Heiles, C., Peek, J. E. G., Goldsmith, P. F., Koo, B.-C., Krčo, M., Lee, J.-J., Mock, J., Muller, E., Pandian, J. D., Parsons, A., Tang, Y., & Werthimer, D. 2006, *ApJ*, 653, 1210
- Stanimirović, S., Staveley-Smith, L., Dickey, J. M., Sault, R. J., & Snowden, S. L. 1999, *MNRAS*, 302, 417
- Sternberg, A., McKee, C. F., & Wolfire, M. G. 2002, *ApJS*, 143, 419
- Wakker, B. P. & van Woerden, H. 1991, *A&A*, 250, 509
- Wannier, P. & Wrixon, G. T. 1972, *ApJ*, 173, L119
- Wolfire, M. G., McKee, C. F., Hollenbach, D., & Tielens, A. G. G. M. 1995, *ApJ*, 453, 673
- Yoshizawa, A. M. & Noguchi, M. 1999, in *IAU Symp. 186: Galaxy Interactions at Low and High Redshift*, Vol. 186, 60